Open access • Journal Article • DOI:10.1117/1.OE.59.4.046106

Comprehensive optical and electrical characterization and evaluation of organic light-emitting diodes for visible light communication — Source link

Zahra Nazari Chaleshtori, Andrew Burton, Stanislav Zvanovec, Zabih Ghassemlooy ...+1 more authors

Institutions: Czech Technical University in Prague, Northumbria University

Published on: 01 Apr 2020 - Optical Engineering (SPIE-Intl Soc Optical Eng)

Topics: Visible light communication, Light-emitting diode, Optical communication and OLED

Comprehensive optical and electrical characterization and evaluation of organic light-emitting diodes for visible light communication

Zahra Chaleshtori, Andrew Burton, Stanislav Zvanovec, Zabih Ghassemlooy, Petr Chvojka

Comprehensive Optical and Electrical Characterization and Evaluation of OLEDs for VLC

Zahra Nazari Chaleshtori,[a] Andrew Burton,[b] Stanislav Zvanovec,[a] Zabih Ghassemlooy,[b] and Petr Chvojka[a]
[a]Czech Technical University in Prague, Faculty of Electrical Engineering, Department of Electromagnetic Field, Technická 2, Prague, Czech Republic, 16627
[b]Northumbria University, Faculty of Engineering and Environment, Optical Communications Research Group, Northumberland Road, Newcastle-upon-Tyne, UK, NE1 8ST

Abstract. In recent years, we have seen an increased use of organic light emitting diodes (OLEDs) for illumination in indoor environments due to the softer light compared with the conventional inorganic LEDs. In addition, OLEDs have been reported in visible light communication (VLC) systems, specifically for applications with lower data rates such as information boards, camera communications and positioning. However, OLEDs need extensive electrical and optical characterization if they are going to be fully exploited in VLC. This paper investigates characteristics of a range of flexible and rigid OLEDs and compares them with inorganic LEDs. We show that, OLEDs have highly linear power-current characteristics, and compared with rigid OLEDs with beam patterns closely matching Lambertian profile, the flexible OLED's radiation pattern is wider than Lambertian. Based on the measured experimental data, a new expression for the OLED's beam pattern, which follows the 3-term Gaussian profile, is proposed. Moreover, we show that using larger size OLED in VLC links offers improved bit error rate performance over a wide tilting angle up to 80° and a transmission path length up to 60 cm.

Keywords: organic LEDs; radiation pattern; spectrum; visible light communications.

Author E-mail: [nazarzah; xzvanove; petr.chvojka] @fel.cvut.cz, [z.ghassemlooy; andrew2.burton] @northumbria.ac.uk

1 Introduction

Visible light communications (VLC) is seen as a viable complementary technology to the radio frequency (RF) wireless communications in mostly indoor environments to meet the growing demands for high-speed wireless data transmission [1, 2]. VLC has the advantages of high energy efficiency (i.e., a green technology), no RF electromagnetic interference, license-free, and has inherent security and privacy compared with the RF technologies [3]. In VLCs, both conventional gallium-based light emitting diodes (LEDs) and organic LEDs (OLEDs) as well as white laser diodes are being used as a light source [1, 4]. The gallium-based LED based VLC systems, which utilize blue light to excite yellowish phosphors to synthesize white light, have been extensively investigated in the literature [1, 5]. Whereas the red, green and blue (RGB) and phosphor laser diodes (LDs) based VLC require higher thermal stability of the phosphor due to a much greater optical power density [6]. Compared with the phosphor-based LD, the RGB LD is safer to the human eye due to the low illumination level blue light component [7].

OLEDs have interesting features over conventional and mainstream solid-state lighting and flat panel displays such as energy efficiency (i.e., they are environmentally friendly), brightness with no need for backlight as in LCD, sunlight style color-temperature tenability, very high color rendering index, small total stack thickness of an OLED being between 100-500 nm [8] and flexibility (i.e., can be used fabricated on plastics substrates or used in wearable clothes) [8-11]. In addition, OLEDs with large photoactive areas are being used as pixels in smartphones, TVs and wearable devices, which offers the potential of infrastructure-to-device (I2D) and device-to-device (D2D) communications [12]. The latter is performed by transmitting and receiving the information data via the smartphone's OLED-based display pixels [13, 14] and the built-in cameras [15, 16].

OLEDs work in a similar manner to LEDs and use organic carbon-based molecules to generate electron-hole pairs but have different characteristics. There are two different types of OLED based on (*i*) small organic molecules deposited on a glass; and (*ii*) polymer (i.e., large plastic molecules) to produce light [17, 18]. However, the modulation bandwidth B_{mod} of OLEDs is orders of magnitude smaller compared with inorganic LEDs (i.e., in the kHz range compared with MHz in inorganic LEDs). The bandwidth limitation is due to the carrier lifetime and the parasitic resistor-capacitor (RC) effects, thus limiting their use in medium- to high-speed data communications [19]. However, OLED properties (i.e., B_{mod}) have been improved by using new materials with higher charge mobility [20]. In addition, a number of advanced communications and signaling schemes as well as optimum driver circuits have been proposed to increase the transmission data rate [21, 22]. Future OLED applications will be in (*i*) medium to large panels for use in public places such as airports, shopping centers, train and bus stations, etc., [23, 24]; and (*ii*) flexible or flat panel display technology for use in wearable biomedical devices in hospitals [25], which provide visual display, data communications and indoor localization. The novel devices of nano-OLEDs and microfluidic OLEDs are promising opening up new applications [26]. However, very little works have been reported on the optical and electrical characterization of different types of standard OLEDs used for illumination, which are essential when these devices are used in VLC. In this paper, we first experimentally investigate optical and electrical characteristics in terms of the threshold voltage, bias current, linear dynamic range, optical spectrum, optical radiation patterns and output optical power-current-voltage (*L*-*I*-*V*) of a number of rigid and flexible (or curved) OLEDs within the context of VLC systems. Additionally, the characterization of organic devices is mostly limited to *L*-*I*-*V* or the frequency response measurements. In this work, the focus also is on other features of OLEDs (particularly large area flexible and rigid devices) such as dynamic resistance, linearity and radiation patterns, which are important in VLC, and compared them with the conventional inorganic sources. Large OLED panels compared with tiny OLEDs have lower modulation bandwidth, thus supporting a reduce level of throughputs in VLC [21, 22]. Therefore, more research utilizing large OLEDs with much lower bandwidth needs to be done. A number of schemes, including multi-carrier and multi-level modulation schemes, have been proposed to increase the data throughput. Here, we demonstrate the use of large size OLEDs as a transmitter in VLC systems employing a multi-band carrier-less amplitude and phase (*m*-CAP) modulation, which offers similar spectrum efficiency as the orthogonal frequency division multiplexing (OFDM) but at much reduced implementation complexity. Hence, we evaluate the system performance in terms of the measured bit error rate (BER).

The rest of the paper is organized as follows. In Section 2, the structure of a typical OLED is described. In Section 3, the characterization of OLEDs is given followed by the experimental investigation of OLED-based VLC link in Section 4, and finally, conclusions are drawn in Section 5.

2 The Structure of OLEDs

The principal material in an organic semiconductor is either carbon or nitrogen [27]. The organic materials can be long-chain polymers (i.e., PLEDs) or small organic molecules (i.e., SMOLEDs) in a crystalline phase [19, 27]. The organic devices are based on the thin-film technology (see Fig. 1), where the general structure consists of two or more organic semiconductor materials sandwiched between oppositely polarized electrodes. OLEDs have a low-pass filter transfer function with the cut-off frequency given by [28]:

$$f_{3\text{-dB}} = \frac{1}{2\pi(\tau_s + \tau_c)}, \tag{1}$$

where τ_s is the differential carrier lifetime, which is inversely proportional to the drive current [28]. $\tau_c \sim RC$, where R is the effective resistance of the OLED and C is the plate capacitance, which is defined as [1]:

$$C = \frac{A\varepsilon_0\varepsilon_r}{d}, \tag{2}$$

where A is the OLED photoactive area, d is the OLED thickness, and ε_0 and ε_r are the permittivity of free space and relative dielectric constant of the organic layer, respectively.

Note that, as in LEDs, B_{mod} of OLEDs is inversely proportional to A, hence much lower bandwidth than small area gallium-based LEDs [4]. In addition, in highly bandlimited organic

VLC systems the inter-symbol interference (ISI) leads to the significant BER degradation. A number of schemes have been proposed to overcome both lower B_{mod} and the ISI including: high-level modulations [29, 30], equalization schemes such as the artificial neural network (ANN) [21, 22], specially designed receivers [31-35], single-input multiple-output (SIMO) or multiple-input multiple-output (MIMO) configuration [36, 37], bit/power loading [22, 38] and power pre-emphasis [30, 39].

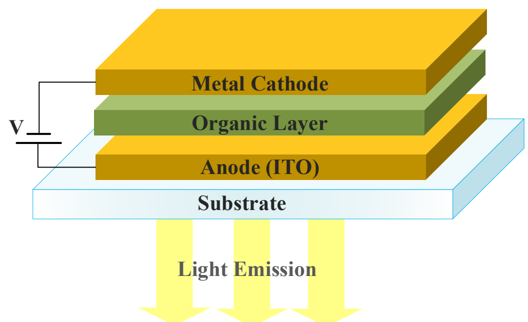

Fig. 1 The OLED structure.

3 Characterization of OLEDs

3.1 Experimental Test-bed

To carry out comprehensive tests and measurements for characterization of the OLEDs, we have developed an experimental test-bed, as shown in Fig. 2. The test-bed includes an arbitrary function generator AFG Agilent 3252, driving circuits, OLEDs, optical receiver (ORx) Thorlabs PDA100A2 (consisting of a photodiode (PD) and a transimpedance amplifier (TIA)), spectrometer Thorlabs CCS200 with CCSB1 cosine corrector with a diameter of 8.5 mm and the digital LED lux meter DT-3809.

Five OLEDs - four different rigid OLEDs from LG (i.e., N6OA40C, N6SC40C, N6BA40C and N6SB40 denoted as D_1 to D_4) and a single flexible OLED from UNISAGA (denoted as D_5), see Fig. 3, were investigated in terms of their optical and electrical characteristics including the optical spectrum, *L-I-V* curves, optical radiation pattern and B_{mod}. All experiments were carried out under the same controlled environments (within a dark room) and for each set-up, five sets of measurements were carried to ensure repeatability and correctness. The main parameters of tested OLEDs are given in Table 1.

Table 1 The OLEDs under test.

OLED	Size (mm)	Device thickness (mm)	Luminous efficiency (lm/W) (Bias current I_B (mA))	Luminous flux (lm) (I_B (mA))
Rigid				
D_1: N6OA40C	48.7 (Radius)	1	55 (230)	75 (230)
D_2: N6SC40C	140 ×140	0.88	55 (480)	150 (480)
D_3: N6BA40C	200 × 50	1.77	53 (230)	73 (230)
D_4: N6SB40	55 × 53	1.97	55 (62)	20 (62)
Flexible				
D_5	200 × 50	0.41	53 (230)	75 (230)

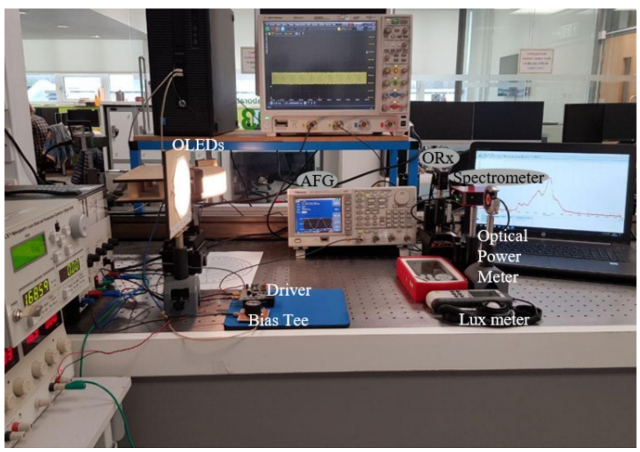

Fig. 2 An experimental test-bed for characterization of OLEDs.

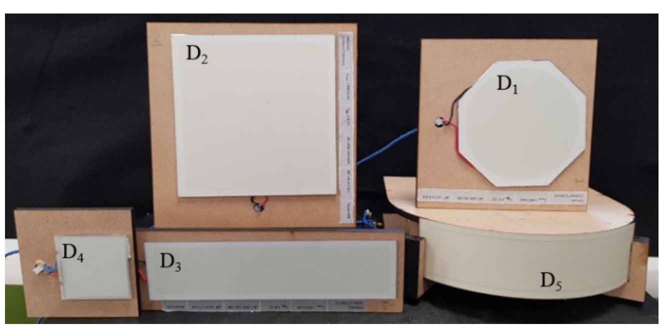

Fig. 3 Different OLEDs (D_1 to D_5) under test.

3.2 Optical and Electrical Characterization

3.2.1 OLED's spectrum

To measure the spectrum profiles of OLEDs, a spectrometer with a cosine corrector capturing light over a 180° angle was used. The measured normalized optical spectrum (averaged over five sets of measurements) for a range of I_B for D_1 is depicted in Fig. 4(a) showing R, G and B components at the peak wavelengths of 613, 555 and 450 and 480 nm, respectively. OLEDs D_1-D_5 and an inorganic white LED (LUXEON cool white rebel star LED (5650K) sr-01) display broad-spectrum profiles with RGB components, see Fig. 4(b). For the flexible OLED, the R component is at a slightly higher wavelength of 620 nm, whereas B and G components have lower intensities compared with the rigid OLEDs. This is attributed to the lower conversion efficiency of B and G materials in D_5. Whereas, for the inorganic LED the dominant color is B.

Next, we investigate the spectrum (i.e., the color) of the D_1 under different dimming levels (i.e., 10 mA < I_B < 300 mA) as shown in Fig. 4(c). Note, the normalized intensity profiles are almost the same with low intensity variation of the peak intensities. Thus, indicating no significant changes in the color of OLEDs in contrast to the inorganic LEDs reported in [40].

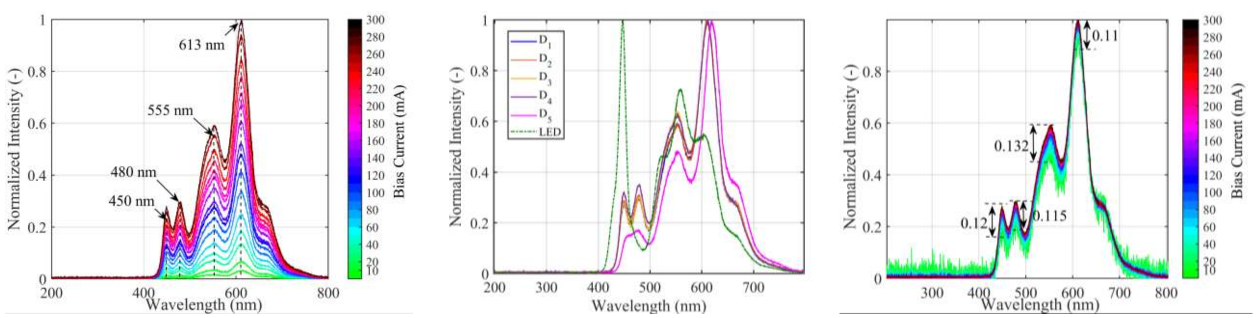

(a) (b) (c)

Fig. 4 (a) The optical spectrum of D_1 are normalized to the maximum I_B with peak wavelengths marked where the legend color scale represents I_B, (b) all devices outputs and a gallium-based white LED at their corresponding maximum I_B, and (c) the optical spectrum of D_1 for a range of I_B where each of the spectral responses were normalized to unity and then superimposed on top of each other.

3.2.2 OLED L-I-V curves

The *I-V* curves of the OLED panels under test were measured using a source meter (Keithley SourceMeter Series 2400) and their illuminance was measured using a lux meter, where the distance between the OLED and the lux meter was fixed at 15 × the horizontal dimension of the OLED (as recommended by lux meter manufacturer). The measured *L-I-V* curves of the OLEDs are illustrated in Fig. 5 showing linear characteristics with sufficient dynamic ranges. Table 2 summarizes the measured maximum current $I_{B\text{-Max}}$, threshold voltage V_{th}, range of I_B in the linear part ΔI, range of voltage in the linear part ΔV and slope of the *V-I* curve (i.e., inverse of the dynamic resistance for all OLEDs at I_B). Note, with a wide linear range *L-I* range around I_B higher signal levels can be used for intensity modulation of the OLED, thus higher signal to noise ratio and lower BER). Using linear regression curve-fitting, the plots in Fig. 5 show a highly linear *L-I* relationship. To compare the linearity of inorganic LEDs with OLEDs we have used root mean square error (RMSE) i.e., $RMSE = \sqrt{(\sum P_I - P_{\text{mod}})^2/n}$, where P_I and P_{mod} are the measured and linear modelled optical powers, respectively and n is the number of measured samples, see Table 3. Note, OLEDs tested in this work show a considerably lower RMSE compared with the inorganic LEDs (i.e., RGB, 5 mm RGB, RAGB (RGB + amber LEDENGIN LZ4-00MA00) and a COBLED (LUSTREON 4W 48led COBLED Chip)).

Table 2 The parameters of OLEDs under test

OLED	$I_{B\text{-Max}}$ (mA)	V_{th} (V)	Slope ($\Delta I/\Delta V$)	Dynamic resistance (Ω) (I_B (mA))
D_1	300	4.6	0.263	3.8 (160)
D_2	800	4.8	0.400	2.5 (400)
D_3	350	4.8	0.225	4.4 (160)
D_4	100	5.0	0.083	12.0 (60)
D_5	300	7.0	0.033	4.3 (180)

Table 3 The parameter of linearity of inorganic LEDs and OLEDs

OLED	RMSE	Ga LED	RMSE		
			R	G	B
D_1	2×10^{-14}	RGB	0.004	0.07	0.008
D_2	3×10^{-14}	RAGB	0.0036	0.0025	0.0032
D_3	1.1×10^{-14}	5 mm RGB	0.0016	0.0027	0.0047
D_4	1.3×10^{-7}	COBLED		0.5114	
D_5	1.2×10^{-14}				

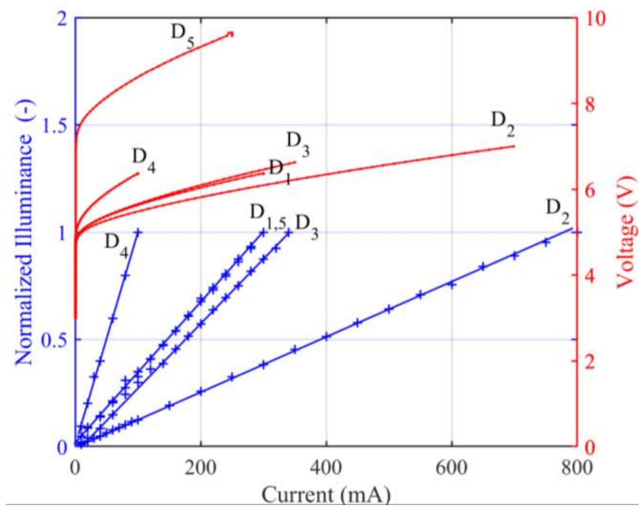

Fig. 5 The *L-I-V* curves for OLEDs where *V-I* and *L-I* curves are associated to each device marked as D_1 to D_5.

3.2.3 Optical radiation pattern

The optical radiation pattern describes the spatial intensity distribution of light emitted from the OLEDs, which is important, especially when analyzing the coverage and signal distribution in VLC links. The light intensity of LEDs defined in terms of the angle of irradiance θ is given by [1, 2]:

$$I(\theta) = \frac{m_L + 1}{2\pi} I(0) \cos^{m_L}(\theta), \qquad \theta = [-\frac{\pi}{2}, \frac{\pi}{2}] \tag{3}$$

where $I(0)$ is the center luminous intensity of an LED and m_L is Lambertian order given as [1]:

$$m_L = -\frac{\ln(2)}{\ln[\cos(\theta_{1/2})]}, \tag{4}$$

where $\theta_{1/2}$ is the semi-angle at half illuminance.

In order to empirically derive the beam patterns of rigid OLEDs and determine Lambertian order of emission, a lux meter was used to measure the luminance, as shown in Fig. 6(a). As expected, the profiles are complete hemispheres close to Lambertian emitter with $m_L = 1$ in contrast to the intensity profile of a COBLED with $m_L = 0.66$ as shown in Fig. 6(b).

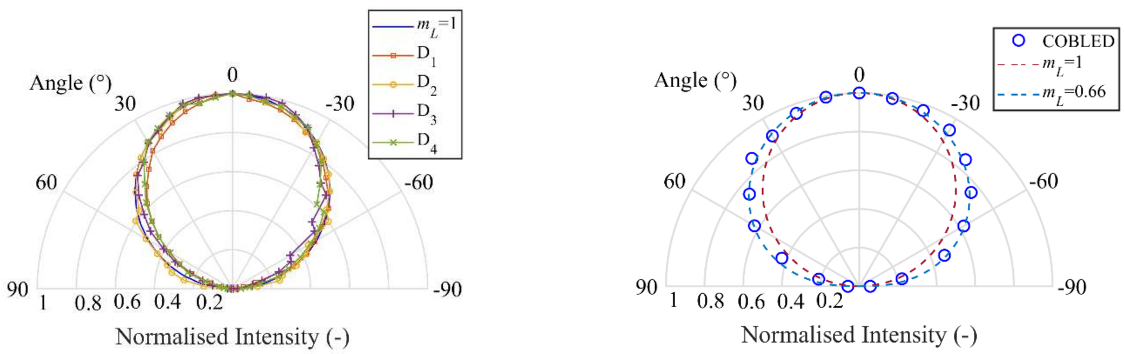

(a) (b)

Fig. 6 The polar dimensional radiation patterns for: (a) rigid OLEDs for D_1, D_2, D_3, and D_4 and (b) a COBLED.

With reference to Fig. 7(a), the irradiance angle θ is given as:

$$\theta = \arccos \frac{\vec{d}_{Rx} . \vec{r}_{\mathrm{OLED}}}{\left|\vec{d}_{Rx}\right| \left|\vec{r}_{\mathrm{OLED}}\right|}, \tag{5}$$

where $\vec{r}_{\mathrm{OLED}}$ and $\vec{r}_{\mathrm{Rx}}$ are the norm vectors of the OLED and the ORx, respectively, and d_{Rx} is a distance of OLED and ORx. The position of OLED and the ORx can be considered as (r, φ, x_1) and (r', φ', x_2) in the cylindrical coordinate, respectively, where r is the OLED curvature radius, $0 < \varphi < 180°$ and x_1 refers to the OLED's width. Thus, we have:

$$\cos(\theta) = \frac{r'\cos\varphi'\cos\varphi - r\cos^2\varphi + r'\sin\varphi'\sin\varphi - r\sin^2\varphi}{r' - r}. \tag{6}$$

To investigate the intensity profiles of flexible OLED, the device was bent with the different radius of curvatures r of 11 cm and 8 cm to have quadrature and half-circle light sources, as shown in Fig. 7(a). The measured radiation pattern shows a symmetry about the origin 0° not fitting Lambertian radiation pattern, see the solid blue line for m_L = 1 in Fig. 7(b). Note, the OLED with higher r displays a radiation beam profile closer to Lambertian with m_L = 1. The radiation angle ranges for $\theta_{1/2}$ for the flat 11 and 8 cm curved OLEDs are 58°, 65°, 75°, respectively.

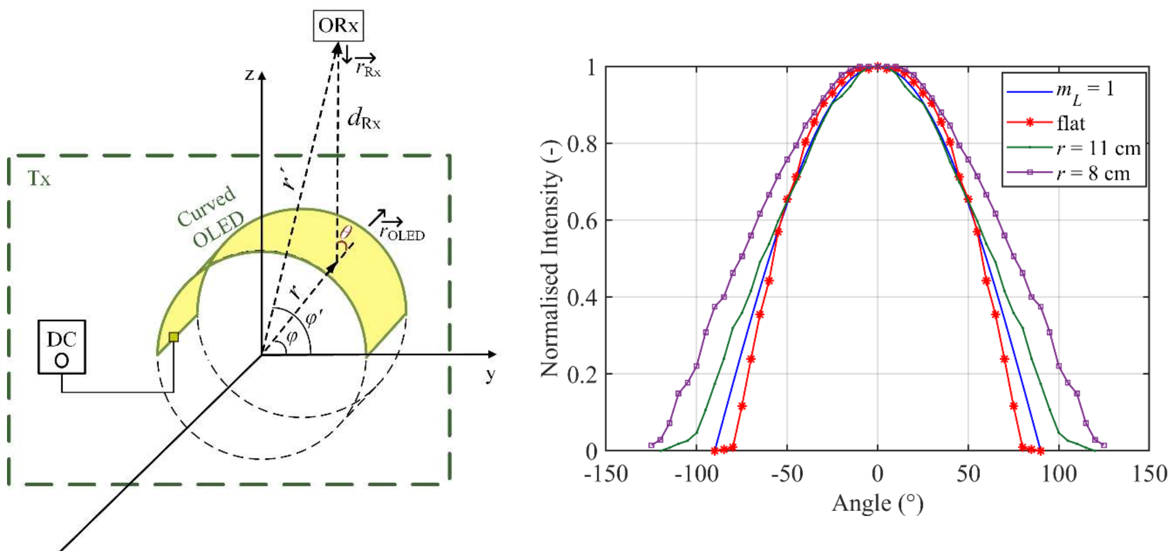

(b)

Fig. 7 (a) OLED panel bent in different curvature radius r of 11 and 8 cm and (b) two-dimensional intensity pattern.

A numerical fitting method was used to estimate the radiation pattern parameters of flexible OLEDs. The 3-term Gaussian model provided the best fit to describe the radiation patterns of OLEDs, which is given by:

$$I(\theta) = \sum_{k=1}^{q} a_k \times exp\left(-\left((\theta - b_k)/c_k\right)^2\right), \quad (7)$$

where a_k, b_k, c_k, are parameters estimated by the curve fitting tool, k is the order and q is the term of Gaussian model, which is considered to be 3 for the best match with the empirical data. The RMSE analysis has been carried out on the modelled and measured intensity profiles to assess the accuracy of the model. For the curved OLED, the RMSE values are 0.016 and 0.018 for r of 11 and 8 cm, respectively, which are less than the standard error limit of 0.05 [41]. The numerical fitting parameters are shown in Table 4 for OLEDs with r of 11 and 8 cm. Note, a_k is the peak of the k^{th} term of 3-term Gaussian (i.e., $a_1 \sim 1$), and b_k is the angular position of peak referred to the each Gaussian as $b_1 \sim 0$. c_k is the standard deviation of the k^{th} term of the 3-term Gaussian with higher values representing a wider profile.

Table 4 3-term Gaussian model parameter for spatial intensity distribution for curvature with a radius of 11and 8 cm

k	**1**	**2**	**3**
	***r* = 11 cm**		
a_k	0.9878	0.3054	0.2875
b_k	-0.7595	58.1	-59.42
c_k	51.59	32.99	31.94
	***r* = 8 cm**		
a_k	0.9814	0.3733	0.2721
b_k	4.832	-63.31	70.73
c_k	60.17	42.31	36.66

3.2.4 OLED bandwidth

To measure B_{mod} of the OLEDs, the devices were biased in the linear region of respective *L-I* curves, see Fig. 5. The measured frequency responses for D_1-D_5 over a range of I_B are as shown in Fig. 8, where U is the peak-to-peak received voltage and U_0 is the peak-to-peak voltage of the first sample. For comparison, the maximum and minimum bandwidth values as well as the difference between them (i.e., ΔB) are given in Table 5. The results for the devices tested show that, B_{mod} increases with I_B as in agreement with (1). We also investigated the effect of bending the flexible OLED on B_{mod} and observed no changes in B_{mod}. This is because the cut-off frequency of OLED is defined by its physical parameters. This feature makes the OLED a perfect optical antenna, where the same SNR is maintained over a given transmission radius.

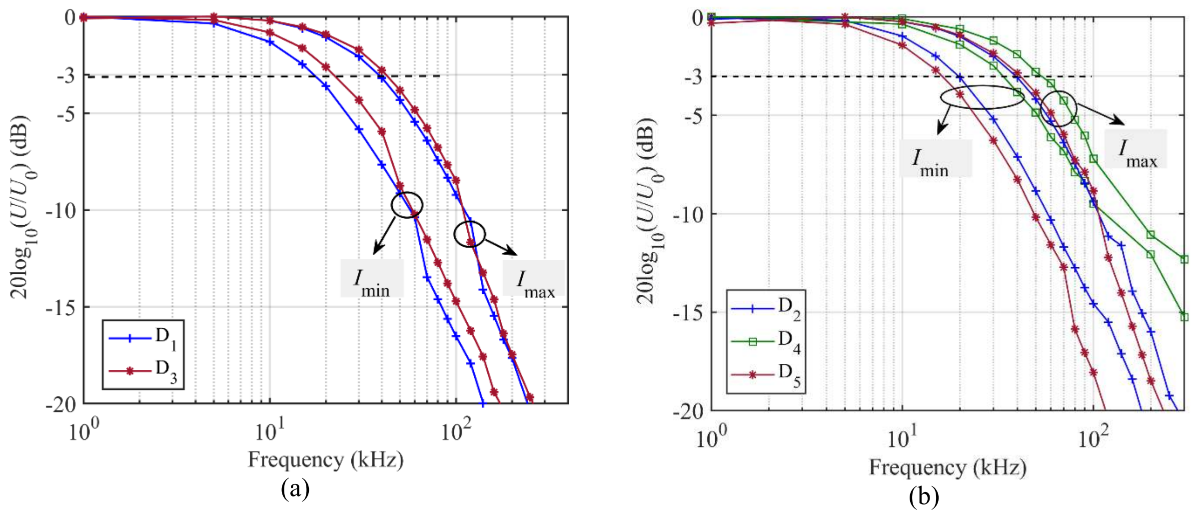

Fig. 8 The measured B_{mod} of: (a) $D_{1,3}$ and (b) $D_{2,4,5}$.

Table 5 Bandwidth of OLEDs

Device	$B_{mod\text{-}Min}$ (kHz) ($I_{B\text{-}Min}$ (mA))	$B_{mod\text{-}Max}$ (kHz) ($I_{B\text{-}Max}$ (mA))	ΔB (kHz)
D_1	15 (40)	38 (250)	23
D_2	20 (100)	40 (600)	20
D_3	20 (100)	42 (280)	22
D_4	34 (30)	54 (60)	20
D_5	15 (40)	42 (250)	27

4 Experimental OVLC Link Results

4.1 Experimental test-bed for OVLC link with m-CAP

OLEDs with both high linearity and dynamic range can be used to support higher-order multi-level and multi-carrier modulation schemes. However, in this work to simply demonstrate the potential of the OLEDs as the transmitter in a VLC system, we have developed an experimental test-bed to assess the link performance. We have adopted *m*-CAP modulation scheme due to (*i*) reducing the effect of the highly bandlimited frequency response of OLEDs acting as a low-pass filter [42-44]; (*ii*) can be used as a multiuser scheme (e.g., personalized advertising) [45]; and (*iii*) implementation simplicity compared with the OFDM.

A block diagram of the experimental m-CAP OVLC link is shown in Fig. 9. Firstly, m independent pseudo-random data streams $d_m(t)$ of length 12,000 bits (memory depth limitation of the AFG) are generated and mapped onto the M-QAM (quadrature amplitude modulation) constellation where M is the order of the QAM. Note, M and m are selected as 16 and 2, respectively, in this work. During the experiment, a sufficient number of bits were transmitted to allow the measurement of the BER at 10^{-6}. The linearity of OLEDs and their high dynamic range offer the potential to choose a number of carriers. Following upsampling, the real and the imaginary parts of the signal a_i and b_i, respectively, are applied to the in-phase and quadrature pulse shaping transmit filters, whose impulse responses form a Hilbert pair (i.e., they are orthogonal in the time domain). The transmit filters are formed as a product of the square root raised cosine (SRRC) filter pulse shapes and the sine and cosine waves for the quadrature and in-phase part of the signal, respectively. The carrier frequencies given by the transmit filters are set to 10 and 30 kHz for 1st and 2nd subcarriers (s_1 and s_2), respectively, in this work. The roll-off factor β used for the transmit pulse shapes is chosen as 0.15, given that the minimum bandwidth requirement is proportional to $1 + \beta$. Note, higher β leads to more protection against ISI for consistency with the literature [46]. The combined output from filters, i.e., m-CAP signal $x(t)$, is applied to AFG and used via a driver for intensity modulation of the OLEDs. Following transmission over a short free space (up to 60 cm) line of sight (LoS) channel, the signal is detected using ORx Thorlabs PDA100A2. Subsequently, the output of ORx is captured using digital storage oscilloscope Keysight DSO9254A with the sampling frequency of 400 kS/s for further off-line data processing. The regenerated electrical signal is given as $y(t) = x'(t) \otimes h(t) + n(t)$ where $h(t)$ is the channel impulse response, the $\otimes$ symbol denotes convolution, and the noise $n(t)$ is mainly due to the ambient light and in the form of shot noise. $y(t)$ is resampled to transmitted signal by original sampling frequency prior to being applied to two time-reversed filters g_I and g_Q matched to the transmit filters. The combined filter output $z(t)$ followed down-sampling are applied to the M-QAM demapper to re-generate the estimates transmitted data $d'_m(t)$. All the key system parameters are shown in Table 6.

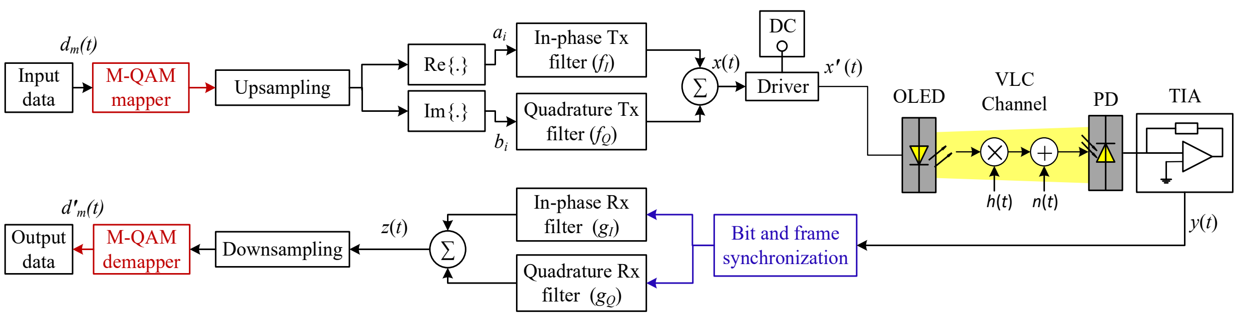

Fig. 9 The block diagram of the proposed OVLC system with m-CAP modulation.

Table 6 The system parameters

OLED	I_B **(mA)**	B_{mod} **(kHz)**	**luminous flux (lm)**	**Area (cm^2)**
D_1	160	28	58.5	74.5
D_2	450	30	115.0	196.0
D_3	160	32	52.0	100.0
D_4	60	54	19.4	29.2
D_5	180	34	68.4	100.0
ORx	**Parameter**	**Value**		
	Type of PD	Si-PIN		
	Active area of PD	75.4 mm^2		
	Bandwidth	1.4 MHz at a 10 dB gain		
	Output voltage	0 to 10 V		
	Noise of amplifier	195 µV (RMS)		
	NEP	6.75×10^{-12} (W/$\sqrt{\text{Hz}}$) at λ= 960 nm		
	Responsivity	0.2 (A/W) at λ= 400 nm 0.5 (A/W) at λ= 700 nm		

4.2 Experimental results

In this section, we evaluate the LoS OLED VLC link based on the BER for a range of transmission span 10 to 60 cm and the OLED tilt angles α from -90º to 90º. The BER results versus the path length for the OLED VLC and for s_1 and s_2 are shown in Figs. 10(a) and (b), respectively along with the 7% forward error correction (FEC) BER limit of 3.8×10^{-3}. Examples of measured constellation diagrams are shown as insets for D_2 with two distance d of 40 and 50 cm and 30 and 50 cm for s_1 and s_2, respectively. At the FEC BER limit, the transmission path lengths for s_1 are 36, 50, and ~60 cm for D_4, $D_{1,3}$ and $D_{2,5}$, respectively, which are sufficient for D2D communications. In the case of s_2, we observe a small decrease in the transmission spans by 2, 15, and 10 cm for D_4, $D_{1,3}$ and $D_{2,5}$, respectively compared with s_1. Although the path length of 60 cm was obtained from our experiment, even longer distances can be achieved using OLED panels made of materials with higher charge mobility giving higher B_{mod} [20, 47] or larger panels with higher output optical power. To meet a given BER target and increase the transmission span, the same SNR at a receiver and thus higher output optical power are required. Therefore,

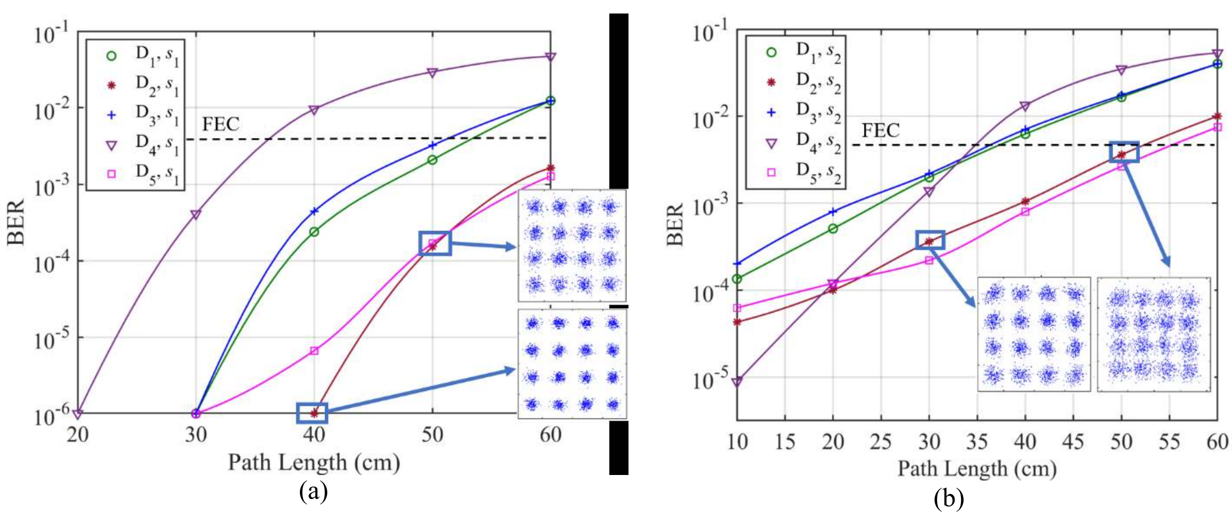

Fig. 10 The BER versus the path length for OLEDs with m-CAP for (a) s_1 with the consolation diagrams for two distance of 40 and 50 cm for D_2 and (b) s_2 with the consolation diagrams for two distances of 30 and 50 cm for D_2.

organic devices with larger area (note decreased 3 dB bandwidth) or an array of OLEDs can be utilized to follow these requirements. For instance, an OLED panel with a luminous flux of ~3000 lm can support data transmission for distances up to 3 m.

For D_2, the BER plots in polar formats against α are shown in Fig. 11 for s_1 and s_2. Also shown for comparison is the plot for the FEC BER limit. Note, the path length is fixed at 30 cm (i.e., a BER < 10^{-6} when $\alpha = 0°$ see Fig. 10(a)). Note, the BER profiles display a symmetry about the origin (i.e., the ORx is facing the OLED at α of 0º) offering improved performance over a wide tilting angle. To meet the FEC limit, D_2 can operate with α up to ±80° and ±70° for s_1 and s_2, respectively.

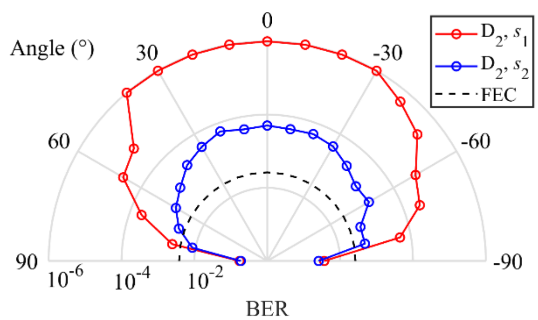

Fig. 11 The polar plot of BER for tilted OLED (D_2) with *m*-CAP for s_1 and s_2.

5 Conclusions and Future Outlook

In this paper, we carried out characterization for a range of fixed and flexible OLEDs in terms of their optical spectrum, power-current and illumination profiles. We showed that, OLEDs offer stable illumination profile regardless of the bias current and a highly linear power-current characteristic compared with the inorganic LEDs. We also showed that, the rigid OLEDs beam pattern closely matches Lambertian with $m_L = 1$, whereas for curved OLED, the radiation pattern displays a symmetry, which is wider than Lambertian as for curved OLED with a curvature radius of 8 cm and a radiation angle of 75°. Based on the measured experimental data for the curved OLED, we showed a new expression for the OLED's beam pattern, which follows the 3-term Gaussian profile with RMSE value of less than a standard error limit of 0.05 to assess the accuracy of the model. In addition, we evaluated OLED-based VLC systems for low data rate transmissions as in D2D communications. We showed the BER results of tilting OLED displayed a symmetry about the origin, with larger size OLEDs showing improved BER (i.e., below the FEC limit) over a wider tilting angle (up to 80°, which is considerably large for D2D communications) and a longer transmission length (i.e., up to 60 cm).

Acknowledgments

This work is supported by the European Union's Horizon 2020 research and innovation programme under the Marie Sklodowska-Curie grant agreement no 764461 (VISION) and the Czech Rep. funded project GACR 17-17538S.

References

[1] Z. Ghassemlooy, L. N. Alves, S. Zvanovec, and M.-A. Khalighi, *Visible Light Communications: Theory and Applications*. CRC Press, 2017.

[2] Z. Ghassemlooy, W. Popoola, and S. Rajbhandari, *Optical wireless communications: system and channel modelling with Matlab®*, 2nd ed. CRC press, 2019.

[3] P. H. Pathak, X. Feng, P. Hu, and P. Mohapatra, "Visible light communication, networking, and sensing: A survey, potential and challenges," *IEEE communications surveys & tutorials,* vol. 17, no. 4, pp. 2047-2077, 2015.

[4] P. A. Haigh *et al.*, "Organic visible light communications: Recent progress," in *2014 16th International Conference on Transparent Optical Networks (ICTON)*, 2014: IEEE, pp. 1-5.

[5] P. Binh and N. Hung, "High-speed visible light communications using ZnSe-based white light emitting diode," *IEEE Photonics Technology Letters,* vol. 28, no. 18, pp. 1948-1951, 2016.

[6] J. Yang *et al.*, "Highly uniform white light-based visible light communication using red, green, and blue laser diodes," *IEEE Photonics Journal,* vol. 10, no. 2, pp. 1-8, 2018.

[7] T.-C. Wu, Y.-C. Chi, H.-Y. Wang, C.-T. Tsai, Y.-F. Huang, and G.-R. Lin, "Tricolor R/G/B laser diode based eye-safe white lighting communication beyond 8 Gbit/s," *Scientific reports,* vol. 7, no. 1, p. 11, 2017.

[8] P. A. Haigh, Z. Ghassemlooy, S. Rajbhandari, and I. Papakonstantinou, "Visible light communications using organic light emitting diodes," *IEEE Communications Magazine,* vol. 51, no. 8, pp. 148-154, 2013.

[9] P. Haigh, "Using equalizers to increase data rates in organic photonic devices for visible light communications systems," University of Northumbria, 2014.

[10] J. Ràfols-Ribé *et al.*, "High-performance organic light-emitting diodes comprising ultrastable glass layers," *Science advances,* vol. 4, no. 5, p. eaar8332, 2018.
[11] J. Clark and G. Lanzani, "Organic photonics for communications," *Nature photonics,* vol. 4, no. 7, p. 438, 2010.
[12] P. Luo, M. Zhang, Z. Ghassemlooy, S. Zvanovec, S. Feng, and P. Zhang, "Undersampled-based modulation schemes for optical camera communications," *IEEE Communications Magazine,* vol. 56, no. 2, pp. 204-212, 2018.
[13] Y. Li, Z. Ghassemlooy, X. Tang, B. Lin, and Y. Zhang, "A VLC smartphone camera based indoor positioning system," *IEEE Photonics Technology Letters,* vol. 30, no. 13, pp. 1171-1174, 2018.
[14] R. Boubezari, H. Le Minh, Z. Ghassemlooy, and A. Bouridane, "Smartphone camera based visible light communication," *Journal of Lightwave Technology,* vol. 34, no. 17, pp. 4121-4127, 2016.
[15] B. Lin, Z. Ghassemlooy, C. Lin, X. Tang, Y. Li, and S. Zhang, "An indoor visible light positioning system based on optical camera communications," *IEEE Photonics Technology Letters,* vol. 29, no. 7, pp. 579-582, 2017.
[16] Q. Wang *et al.*, "Light positioning: A high-accuracy visible light indoor positioning system based on attitude identification and propagation model," *International Journal of Distributed Sensor Networks,* vol. 14, no. 2, p. 1550147718758263, 2018.
[17] J. H. Burroughes *et al.*, "Light-emitting diodes based on conjugated polymers," *nature,* vol. 347, no. 6293, p. 539, 1990.
[18] C. W. Tang and S. A. VanSlyke, "Organic electroluminescent diodes," *Applied physics letters,* vol. 51, no. 12, pp. 913-915, 1987.
[19] Z. H. Kafafi, *Organic electroluminescence*. CRC Press, 2018.
[20] W. Zhu *et al.*, "Graphene radio frequency devices on flexible substrate," *Applied Physics Letters,* vol. 102, no. 23, p. 233102, 2013.
[21] P. A. Haigh *et al.*, "A 20-Mb/s VLC link with a polymer LED and a multilayer perceptron equalizer," *IEEE Photonics Technology Letters,* vol. 26, no. 19, pp. 1975-1978, 2014.
[22] H. Chen, Z. Xu, Q. Gao, and S. Li, "A 51.6 Mb/s Experimental VLC System Using a Monochromic Organic LED," *IEEE Photonics Journal,* vol. 10, no. 2, pp. 1-12, 2017.
[23] T. Yamada, "Latest Development of Soluble-OLED Material and its Application to Mid-to large-sized Panel Production," in *2019 26th International Workshop on Active-Matrix Flatpanel Displays and Devices (AM-FPD)*, 2019, vol. 26: IEEE, pp. 1-4.
[24] H. J. Shin and T. W. Kim, "Ultra-High-Image-Density, Large-Size Organic Light-Emitting Device Panels Based on Highly Reliable Gate Driver Circuits Integrated by Using InGaZnO Thin-Film Transistors," *IEEE Journal of the Electron Devices Society,* vol. 7, pp. 1109-1113, 2019.
[25] J. Smith *et al.*, "Application of flexible flat panel display technology to wearable biomedical devices," *Electronics Letters,* vol. 51, no. 17, pp. 1312-1314, 2015.
[26] T. Kasahara, H. Kuwae, and J. Mizuno, "New Era of Device Science," in *2019 Pan Pacific Microelectronics Symposium (Pan Pacific)*, 2019: IEEE, pp. 1-6.
[27] J. Kalinowski, *Organic Light-Emitting Diodes: Principles, Characteristics & Processes*. CRC press, 2018.
[28] P. Deng, M. Kavehrad, and M. A. Kashani, "Nonlinear modulation characteristics of white LEDs in visible light communications," in *Optical Fiber Communication Conference*, 2015: Optical Society of America, p. W2A. 64.
[29] P. A. Haigh *et al.*, "Wavelength-multiplexed polymer LEDs: Towards 55 Mb/s organic visible light communications," *IEEE Journal on Selected Areas in Communications,* vol. 33, no. 9, pp. 1819-1828, 2015.

[30] S. T. Le *et al.*, "10 Mb/s visible light transmission system using a polymer light-emitting diode with orthogonal frequency division multiplexing," *Optics letters,* vol. 39, no. 13, pp. 3876-3879, 2014.
[31] A. Burton *et al.*, "Optoelectronic Modelling, Circuit Design and Modulation for Polymer-Light Emitting Diodes for Visible Light Communication Systems," in *2019 26th International Conference on Telecommunications (ICT)*, 2019: IEEE, pp. 55-59.
[32] A. Burton, H. Le Minh, Z. Ghassemlooy, S. Rajbhandari, and P. A. Haigh, "Smart receiver for visible light communications: Design and analysis," in *2012 8th International Symposium on Communication Systems, Networks & Digital Signal Processing (CSNDSP)*, 2012: IEEE, pp. 1-5.
[33] Z. Zeng, M. D. Soltani, M. Safari, and H. Haas, "Angle Diversity Receiver in LiFi Cellular Networks," in *ICC 2019-2019 IEEE International Conference on Communications (ICC)*, 2019: IEEE, pp. 1-6.
[34] C. Chen, M. D. Soltani, M. Safari, A. A. Purwita, X. Wu, and H. Haas, "An omnidirectional user equipment configuration to support mobility in LiFi networks," in *2019 IEEE International Conference on Communications Workshops (ICC Workshops)*, 2019: IEEE, pp. 1-6.
[35] M. D. Soltani *et al.*, "Bidirectional Optical Spatial Modulation for Mobile Users: Toward a Practical Design for LiFi Systems," *IEEE Journal on Selected Areas in Communications,* vol. 37, no. 9, pp. 2069-2086, 2019.
[36] N. V. Khanh, P. Q. Thai, N. H. Duy, and N. N. A. Khoa, "Investigation on MIMO OLED VLC System Performance," in *Novel Optical Materials and Applications*, 2018: Optical Society of America, p. JTu5A. 61.
[37] P. A. Haigh *et al.*, "A MIMO-ANN system for increasing data rates in organic visible light communications systems," in *2013 IEEE International Conference on Communications (ICC)*, 2013: IEEE, pp. 5322-5327.
[38] H. Chen *et al.*, "A 1.9 Mbps OFDM-based all-organic visible light communication system," in *2016 IEEE International Conference on Communication Systems (ICCS)*, 2016: IEEE, pp. 1-6.
[39] P. Haigh *et al.*, "Organic visible light communications: Methods to achieve 10 Mb/s," in *2017 IEEE Photonics Conference (IPC)*, 2017: IEEE, pp. 553-554.
[40] M. Dyble, N. Narendran, A. Bierman, and T. Klein, "Impact of dimming white LEDs: Chromaticity shifts due to different dimming methods," in *Fifth international conference on solid state lighting*, 2005, vol. 5941: International Society for Optics and Photonics, p. 59411H.
[41] J. W. Gorman and R. Toman, "Selection of variables for fitting equations to data," *Technometrics,* vol. 8, no. 1, pp. 27-51, 1966.
[42] P. A. Haigh *et al.*, "Multi-band carrier-less amplitude and phase modulation for bandlimited visible light communications systems," *IEEE Wireless Communications,* vol. 22, no. 2, pp. 46-53, 2015.
[43] P. A. Haigh *et al.*, "A multi-CAP visible-light communications system with 4.85-b/s/Hz spectral efficiency," *IEEE Journal on Selected Areas in Communications,* vol. 33, no. 9, pp. 1771-1779, 2015.
[44] P. Chvojka *et al.*, "On the m-CAP performance with different pulse shaping filters parameters for visible light communications," *IEEE Photonics Journal,* vol. 9, no. 5, pp. 1-12, 2017.
[45] M. M. Merah, H. Guan, and L. Chassagne, "Experimental Multi-User Visible Light Communication Attocell Using Multiband Carrierless Amplitude and Phase Modulation," *IEEE Access,* vol. 7, pp. 12742-12754, 2019.
[46] M. I. Olmedo *et al.*, "Multiband carrierless amplitude phase modulation for high capacity optical data links," *Journal of Lightwave Technology,* vol. 32, no. 4, pp. 798-804, 2013.
[47] K. Yoshida *et al.*, "245 MHz bandwidth organic light-emitting diodes used in a gigabit optical wireless data link," *Nature Communications,* vol. 11, no. 1, pp. 1-7, 2020.

Biographies

Zahra Nazari Chaleshtori received her MSc degree in 2016 from Isfahan University of Technology, Iran. Now, she is a PhD candidate at Czech Technical University (CTU) in Prague, Czech Republic. She is focused on the utilization of organic LED-based visible light communications for device-to-device. She is involved in EU H2020 Marie Sklodowska-Curie Innovative Training Network (VisIoN 764461) and also a member of Wireless and Fiber Optics team at CTU.

Andrew Burton received the BEng (Hons.), MSc degrees (distinction) and PhD from Northumbria University, UK. Since graduation he worked as Research Fellow at Northumbria University until 2019, when he joined ISOCOM company as a Technical Manager. His research interests include electronics, optical communications and visible-light communications.

Prof. Stanislav Zvanovec received the M.Sc. and Ph.D. degrees from the Czech Technical University (CTU) in Prague, in 2002 and 2006, respectively. He is a Full Professor, the Deputy Head of the Department of Electromagnetic Field and leader of Wireless and Fiber Optics team at CTU. His current research interests include FSO and fiber optical systems, VLC, RF over optics. He is author of two books and more than 250 journal articles and conference papers.

Prof. Zabih Ghassemlooy FOSA, FIET, SMIEEE: BSc(Hons.) EE Engineering, Manchester Metropolitan Univ., (1981), MSc (1984) and PhD (1987), Manchester Univ., UK. 1987-88 Post-Doctoral Research Fellow, City Univ., UK. 2004-14 Associate Dean Research, Faculty of Eng. & Env., Northumbria Univ. Head of Optical Communications Research Group. Research Fellow(2016) and Distinguished Professor(2015), Chinese Academy of Science. 850 publications. Research: optical wireless communications, free space optics, visible light communications. Chief Editor: British J. of Applied Science and Technology.

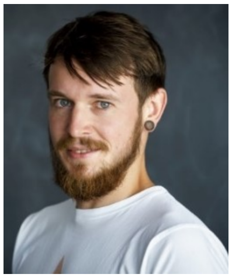

Petr Chvojka received M.Sc. and Ph.D. degrees from the Faculty of Electrical Engineering, Czech Technical University (CTU) in Prague, in 2013 and 2018, respectively. He currently works as a Research Fellow at the Department of Electromagnetic Field, CTU in Prague, where he is a member of the Wireless and Fiber Optics Group. His research focuses on optical systems design and modelling, including inorganic and organic devices and digital signal processing techniques for visible light communications.